Eur. Phys. J. B **34**, 179–192 (2003)
DOI: 10.1140/epjb/e2003-00210-8

THE EUROPEAN PHYSICAL JOURNAL B

EELS study of interfaces in magnetoresistive LSMO/STO/LSMO tunnel junctions

L. Samet[1,3], D. Imhoff[1,a], J.-L. Maurice[2], J.-P. Contour[2], A. Gloter[1], T. Manoubi[3], A. Fert[2], and C. Colliex[1]

[1] Laboratoire de Physique des Solides[b], bâtiment 510, Université Paris-Sud, 91405 Orsay, France
[2] UMR de Physique CNRS/Thalès, Domaine de Corbeville, 91404 Orsay, France
[3] LPMC, Faculté des Sciences de Tunis, Campus Universitaire, 1060 Tunis, Tunisia

Received 3 January 2003 / Received in final form 14 April 2003
Published online 4 August 2003 – © EDP Sciences, Società Italiana di Fisica, Springer-Verlag 2003

Abstract. A magnetic tunnel junction consists of two ferromagnetic conducting electrodes separated by an insulating thin layer. The performance of such a system strikingly depends on the last conducting atomic layers in contact with the insulator. Consequently, the present paper reports a nanoscale electron energy loss spectroscopy (EELS) study, which has been performed across a couple of $La_{0.66}Sr_{0.33}MnO_3$,/$SrTiO_3$/$La_{0.66}Sr_{0.33}MnO_3$ tunnel junctions with different barrier thicknesses (1.5 nm and 5 nm respectively). It aims at determining not only the chemical composition in the interface areas, but also the effect of the neighbouring atoms on their electronic structure. Using recent improvements in the STEM-EELS data acquisition and processing techniques (systematic use of spectrum-line and spectrum-image modes, multivariate statistical analysis, 2D energy deconvolution schemes, etc.), the local chemical information is better extracted with shorter acquisition times, while the large increase of the data set contributes to validate the results. Within the accuracy level of these measurements, the elemental composition of the different phases remains stable up to the interfaces with no evidence of extra doping. Furthermore, weak changes on the Mn-2p edge fine structures (weak shift to lower energy loss values and extra splitting on the top of the Mn L_3 line are observed on all the interfaces. They are interpreted as a consequence of a slight reduction of the local Mn valence likely accompanied by a strain induced change in local symmetry. The discussion is focussed on all spectral changes identified at a (sub)nanometer scale and their potential effects on the degradation of magnetic and transport properties measured, close to room temperature, at a macroscopic level.

PACS. 75.45.+j Macroscopic quantum phenomena in magnetic systems – 82.80.Pv Electron spectroscopy (X-ray photoelectron (XPS), Auger electron spectroscopy (AES), etc.) – 68.37.Lp Transmission electron microscopy (TEM) (including STEM, HRTEM, etc.) – 85.30.Mn Junction breakdown and tunneling devices (including resonance tunneling devices)

1 Introduction

In the present work, we investigate, at a subnanometer scale, the chemical and electronic structure of a magnetoresistive tunnel junction composed of a $La_{1-x}Sr_xMnO_3$ (LSMO "top" layer) / $SrTiO_3$ (STO barrier) / LSMO ("bottom" layer) / STO (substrate) sequence. Indeed, the perovskite-type LSMO system is known to exhibit a variety of physical properties depending on the stoichiometry and on the electronic structure of the Mn ion. For instance, the end member $LaMnO_3$ (LMO) is an "A-type" antiferromagnetic insulator accompanied by a Jahn-Teller distorsion of the Mn^{3+} ion. When the formal valence is increased up close to 4+ for $La_{0.1}Sr_{0.9}MnO_3$, (named in this paper "SMO"), the compound becomes a "G-type" antiferromagnetic insulator in which the nearest-neighbour Mn ions have opposite spins [1,2]. In the intermediate composition range $0.2 < x < 0.6$, the system is a ferromagnetic metal below the Curie temperature which is 370 K for $x = 0.33$ (La/Sr= 2). Zener [3] and subsequently de Gennes [4] explained qualitatively the conductivity of this oxide by the so-called "double-exchange" mechanism. Spectroscopic studies have confirmed that the ground state of LMO is made of a strong mixture of d^4 and $d^5\underline{L}$ where $\underline{L}$ notes for a ligand hole and that the ground state of "SMO" consist of a mixture of d^3 and $d^4\underline{L}$ configuration.

When considering highly efficient candidates for future spin electronics ("spintronics"), most adequate materials for spin dependent switching are the half-metallic ferromagnets, which are expected to exhibit a complete spin polarization of their electron states at the Fermi level.

[a] e-mail: imhoff@lps.u-psud.fr
[b] UMR CNRS 8502

Record magnetoresistances (MR) have been measured in tunnel junctions with electrodes made of half-metallic manganites such as LSMO or $La_{0.7}Ca_{0.3}MnO_3$ (LCMO) separated by a thin insulating layer [5–14]. Large magnetoresistance ratios (400% to 450%) were obtained at low temperature for three insulators epitaxially compatible with LSMO: STO, $PrBa_2Cu_{2.8}Ga_{0.2}O_7$ and CeO_2 [15]. The best characteristics were obtained with the STO barrier. But, disappointingly, these huge MR effects decrease as a function of temperature more rapidly than it could be expected from the value of the Curie temperature (T_c) in the bulk materials. In spite of improvements in growth and device processing, the Curie temperature remains about 90 K below the corresponding value in the bulk. The problem of the influence of the LSMO/STO interface structure has already been discussed in several publications [6,16–19]. Strain, presence of defects, roughness, oxygen stoichiometry, doping amount (La to Sr ratio) can affect the properties of these manganites. In the case of superlattices, Izumi *et al.* [16] have particularly put forward the influence of the sequence of atomic planes at the interface between the manganite and the insulating barrier.

Due to the exponential decay of the tunneling current with distance, the performance of such a system strikingly depends on the last conducting atomic layers close to the insulator. This sequence could be different on each interface in a system with two LSMO electrodes. To test independently the contribution of each interface on electronic properties, the LSMO "top" layer has been substituted by a Co layer [6,20]. While the MR in a Co/STO/LSMO junction is smaller at low temperature than in junctions with two LSMO electrodes (as expected from the moderate polarization of Co in comparison with LSMO), it decreases more slowly at high temperature and vanishes at about 320 K, that is only 50 K below the $T_c^{\rm bulk}$. In this context, a detailed analysis of the nature and the environment of the atoms located at these oxide/oxide interfaces appears extremely relevant for potential applications.

Quite a few investigations of these heterostructures by High Resolution TEM (HRTEM), have been performed over the past years [21–24]. Recently, the $Co/STO/LSMO/STO_{substrate}$ system has been studied jointly with HRTEM and Electron Energy Loss Spectroscopy (EELS), in order to compare the chemical composition, the electronic states and the structural aspects of the interfaces [25]. HRTEM experiments have demonstrated the continuity of the perovskite stacking sequence across the STO/LSMO interface and its abruptness. However, the comparison between HREM images and contrast simulations did not allow to determine what is the atomic termination at the interface. We recall that the termination could be a $La_{2/3}Sr_{1/3}O$ or a MnO_2 monolayer on the LSMO side followed respectively by a TiO_2 or a SrO monolayer on the STO side [25]. The difference in contrast between MnO_2 and TiO_2 was too weak in the HREM experimental images to clearly identify these terminations. EELS experiments in a Scanning TEM (STEM) carried out on the only LSMO/STO interface have demonstrated that the Mn valence did not increase into the last MnO_2 planes at the interface with the STO barrier, so that the most plausible termination corresponds to the "$La_{2/3}Sr_{1/3}O$-TiO_2"-type [25]. The present paper describes the second step of the chemical investigations focusing on the system with two manganite electrodes. We try to elucidate the contribution of each LSMO/STO interface to the reduction of the performance, as compared to the ideal characteristics of such a device. In particular, do the chemical composition and the electronic structure (Mn, O atoms) of the "bottom" LSMO/STO interface differ from the "top" one or/and from the "bulk" LSMO layers?

The specimen preparation, the experimental methods and data processing techniques for chemical characterization are described in Section 2. In Section 3, we present the EELS results (elemental composition and fine structure study). In Section 4, likely diagnoses concerning the environment and valence of the Mn ions at the interfaces are inferred from these results and discussed in the context of the performance of these tunnel junctions.

2 Materials and methods

2.1 Specimen preparation

The LSMO/STO/LSMO tunnel junctions have been grown by pulsed laser deposition (PLD) on a STO substrate [15], at a temperature of 970 K and under a pressure of 0.35 torr of pure oxygen. The growth direction of the LSMO layers was ⟨001⟩. The sample was then cooled to room temperature over a period of 45 mn including an intermediate temperature plateau at 670 K during 15 mn under 300 torr of oxygen to maintain the stoichiometry of the whole device. Two samples which differ in terms of barrier thickness (1.5 nm wide and 5.5 nm wide) have been elaborated. The thinner one corresponds to the specimen on which magnetic and transport measurements have been performed, while the thicker one has been specially prepared for the present EELS study to make sure that the probe in the middle of the barrier would deliver a pure STO reference signal (see below Sect. 3.2.1).

Then, the multilayer specimens have to be thinned so that the interfaces are oriented parallel to electron beam in the TEM (cross-sections). The ultimate alignment is achieved with the tilting mechanisms of the specimen stages of both microscopes. Mechanical thinning using the "tripod method" [26] has constituted the first step in TEM sample preparation while ion milling in a PIPS-Gatan instrument set at low angle and low voltage, was the last one.

2.2 Subnanometer investigations

2.2.1 Nanoscale EELS analysis

The atomic structure of the LSMO/STO/LSMO samples has been investigated by HRTEM experiments

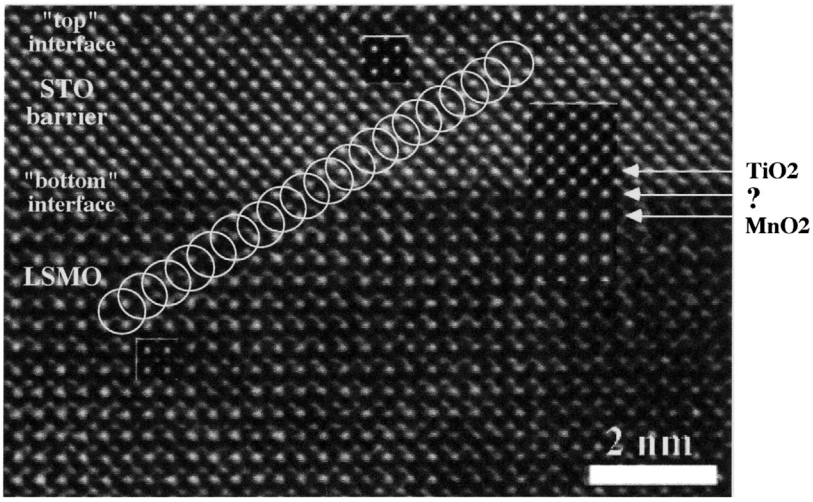

Fig. 1. HREM picture of the STO/LSMO interfaces showing the epitaxial relationship between the two layers. The insets correspond to the calculated contrast with the same focus conditions. The white circles schematically indicate the probe positions during the EELS line spectra. STEM probe diameter is 0.7 nm and the probe step can be reduced down to 0.3 nm.

combined with image simulations (multislice method [27]). HRTEM images of cross-sections have been recorded with a TOPCON EM 002B ($C_s = 0.4$ mm) operated at 200 kV and the details of this structural study are published separately [28,29]. The elemental composition and the electronic structure of the interfaces have been studied in a VG STEM HB501 with a cold field emission gun operated at 100 kV. These measurements have been performed strictly over the same specimen areas as those investigated by HRTEM. EELS data were acquired with a GATAN parallel EELS spectrometer, modified in the laboratory [30]. The latest modification concerns the detector with the installation of a new CCD camera with 1340×100 pixels. This improvement, incorporating also a glass lens coupling between scintillator and CCD chip, has been quite efficient to decrease the acquisition time per spectrum. Acquisition time for each spectrum can be reduced down to 1 ms to few ms in the low energy loss area (below about 150 eV) and down to 10 ms to 200 ms in the core-loss domain (below 1 keV). Also, the calibration makes possible to label the EELS intensity axis in terms of electron numbers rather than counts (see figures). Even in the core-loss domain, these new conditions combined with the spectrum-image technique [31], allow to scan the probe along one ("1D" mode) or two-dimensions ("2D" mode) and to acquire one spectrum per each pixel at very high magnification (up to 5 million).

Major EELS experimental conditions were set as follows: probe size of 0.7 nm (corresponding to 70% of the total primary beam), probe step between each position can be decreased down to 0.3 nm, energy dispersion has been selected between 0.15 eV and 0.5 eV depending on the kind of measurements Energy Loss Near Edge Structure (ELNES) or elemental composition). "1D" spectrum-images consist of 128×1 to 1024×1 spectra and "2D" spectrum-images typically of 64×64 spectra or 128×16 spectra. The very small probe step between two successive positions provides a very large number of energy loss spectra in the same specimen area, very favourable to validate the results. With the "1D" mode, the probe was guided at an angle comprised between 20° to 45° across the interfaces to decrease the interface-probe distance between two successive probe steps (Fig. 1). The energy resolution of about 0.6 eV is mostly limited by the natural energy width of the incident electrons, by spectrometer aberrations and by high tension instabilities. As an example of the energy stability of our system, we have measured in similar conditions, a standard deviation of $+/-0.1$ eV for 200 measurements of the zero loss peak maximum position over a cumulative time of 1 s. Specimen drift is insignificant for the acquisition times used.

2.2.2 EELS data processing

For this study, the selected edges are Sr-4p (31.5 eV), Ti-3p (40 eV), Mn-3p (50 eV), La-4d (117 eV), Sr-3p (133 eV) in the low loss region and Ti-2p (456 eV), O-1s (532 eV), Mn-2p (640 eV) and La-3d (832 eV) in the core-loss region. The Mn-2p and O-1s edges are the main characteristic signals for the fine structure study. Except for the first three mentioned edges in which case the second energy derivative mode is used for quantitative measurements, the continuous background under the edges must be removed by using a smooth power law [32].

Multivariate Statistical Analysis (MSA) is a powerful complementary tool to the spectrum-image technique. The data stored during acquisition of a spectrum-image are considerably increased, which requires a systematic use of statistical tools [33,34]. With a field of use extending beyond noise reduction, MSA keeps the information along space and energy axes as well as it increases the detection

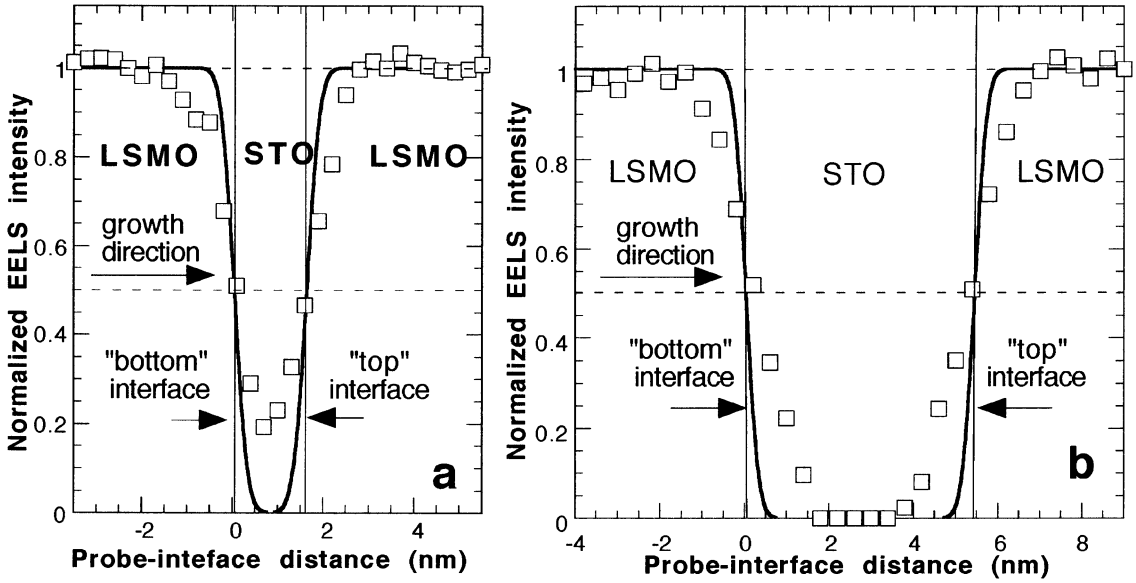

Fig. 2. Typical Mn distribution profile across the STO barrier (a) 1.5 nm and (b) 5.5 nm wide. Theoretical profiles calculated from a convolution with a Gaussian curve is represented (bold line). The probe diameter is 0.7 nm and corresponds to 70% of the signal The acquisition time for each spectrum was 100 ms.

sensitivity of weak feature variations on the characteristic edges. We have also used during the present study a recently developed energy deconvolution technique [35]. This method involves a measurement of the Point Spread Function (PSF) corresponding to the spectrometer aberration, the energy spread of the electron source and the CCD PSF in order to restore the spectrum.

The elemental quantification is based on the potential of the spectrum-image technique, which ensures, with our instrument, very stable conditions during the whole spectral acquisition and large redundancy of information for a same sample area. Since the first purpose of this study is to analyse the interfaces with the STO barrier, the most accurate and simple method consists in monitoring whether an elemental composition is stable over the whole phase area or it varies in particular close to the interfaces. Atomic composition of the layers with optimal accuracy requires an experimental determination of the cross-section ratios from measurements on stoichiometric samples of well known chemical composition [32]. The STO substrate, present in cross sections and a stoichiometric LMO sample were used as references to determine the chemical composition of the different layers. LSMO sample rich in Sr (Sr $>$ 0.6) cannot be used as reference due to their nonstoichiometric composition. The error bars displayed on the elemental profiles have been estimated using the signal to noise ratios (SNR) extracted for each characteristic signal.

As in other transition metals, the Mn-2p edge is the superposition of a continuum and of two white-lines L_3 and L_2. It has been shown that the I_{L3}/I_{L2} intensity ratio can be related to the nominal 3d occupancy on the ion site [36]. We have therefore extracted this ratio using a method described elsewhere [37]. On the other hand, we have determined reference ratios from the standard samples. The whole set of data have been handled with the same procedure in order to minimize the errors, in particular those induced by the choice of the onset position of the continuum relative to the white lines.

3 Results

3.1 Atomic structure in the different layers and at interfaces

Figure 1 shows a HRTEM image of a typical cross section of the LSMO/STO/LSMO films grown along the $\langle 100 \rangle$ direction. It confirms the continuity of the perovskite stacking sequence across the interfaces and its abruptness. Both the LSMO films and the STO barrier are well crystallized without dislocations or other visible extended defects. As a matter of fact, the layer thickness has been previously optimized to avoid the growth of such defects. As already mentioned, the atomic plane terminations "MnO_2-$La_{0.66}Sr_{0.33}O$-TiO_2-SrO" and "$La_{0.66}Sr_{0.33}O$-MnO_2-SrO-TiO_2" at the LSMO/STO interface cannot be distinguished (insets in Fig. 1).

3.2 EELS elemental analysis across the interfaces

3.2.1 About spatial resolution in the EELS experiments?

Figure 2 shows why a specimen with a thicker barrier has specifically been elaborated for the EELS study. It shows the Mn profile in the interfacial areas and across the STO layer for both samples, with tunnel barriers respectively of 1.5 and 5.5 nm nominal thickness. Due to

their major role in the magnetic and transport properties, Mn atoms should not be found in the STO barrier. The first analysis on the sample with a barrier 1.5 nm wide reveals that the Mn-2*p* edge intensity does not completely fall down to zero (Fig. 2a) as well as the La-3*d* edge (not displayed). One can legitimately wonder whether geometrical parameters defining the volume of signal generation (probe spatial distribution, convergence angle, broadening effect and slight misorientation) can satisfactory account for this observation or a real cation interdiffusion in the barrier should be considered. Similar smoothing effects on elemental profiles acquired across SMO/LMO multilayer sequences (the La signal does not go down to zero in the centre of a 2 nm thick SMO layer) have been observed when using a smaller probe diameter of nominal 0.2 nm diameter [38,39]. Figure 2b demonstrates that in the case of the thicker STO barrier, the Mn profile in STO quite falls down to zero. However, the decay of the Mn signal extends over a larger distance (typically between 1.1 nm and 1.8 nm for the d_{20-80} edge criterion), than that expected for an incident probe of nominal 0.7 nm diameter, see the difference between the experimental points and the continuous line representing a step function convoluted by a 2D Gaussian function containing 70% of the total current within a diameter of 0.7 nm [40]. This can be, at least partially, accounted for by beam broadening and convergence angle effects for a local specimen thickness between 30 nm and 40 nm at the position of the analysis. Furthermore, when comparing individual line profiles and summed line profiles across a junction (see for instance Fig. 4a), we have generally noticed a slight further broadening to be interpreted in terms of moderate interface roughness when integrated over distances of a few tens of nanometers within the plane of the interfaces. Consequently, the presently observed loss of resolution induced by the specimen itself cannot allow us to exclude completely the possibility of a slight interdiffusion over one or two atomic planes. Nevertheless, we are convinced that all the cation profiles presented below and the HRTEM images plead for a quite reduced interdiffusion effect, if any.

3.2.2 Cation and anion distribution across the junction

Typical profiles of all involved cations and anion distributions across the junction with the "thick" STO tunnel barrier, are shown in Figure 3 as a function of the probe position. With such a large number of point analyses available, we can study the homogeneity of the measurements over areas normally identified as "bulk" and investigate in more detail the behaviour of the different elemental transitions when the probe approaches and crosses one or the other of the interfaces. The composition of the various ions in the different "bulk" layers remains rather stable. Furthermore, the composition of the STO barrier is strictly identical to that of the substrate (not shown). Contrary to manganese, lanthanum and titanium, oxygen must be present in same proportions in the LSMO and STO layers (3 anions for 2 cations), assuming that the LSMO layers are stoichiometric and relying on identical structural parameters previously measured from HRTEM images [25].

Normalized to 100%, the chemical composition, averaged over the whole "bulk" LSMO layers and excluding the interface areas, is calculated to be: La 13.4 ± 0.2 at%, Sr 6.8 ± 0.2 at%, Mn 20.1 ± 0.3 at% and O 59.7 ± 0.4 at%. The mentioned errors correspond to the standard deviation for more than 100 analysis points. If we assume a perfect stoichiometry of the STO barrier (as a consequence of the similarity with the STO substrate), the corresponding chemical formula for the "bulk" LSMO layers is $La_{0.66}Sr_{0.34}Mn_{0.99}O_{2.95}$. For each measurement shown in Figure 3, the error bars, estimated from the SNR on the characteristic edges, are slightly higher than the statistical variations measured over a large area. Consequently, we can conclude that spatial inhomogeneities of up to 2 or 3 at% on the Sr, La and Mn profiles, can be detected within these "bulk" compounds. If we take into account only the statistical error, a very slight oxygen understoichiometry is revealed in the "bulk" LSMO layers. Of the order of 3%, it must be considered as a likely tendency and should be considered with caution. Using these results, the corresponding Mn valence in the LSMO layers would be 3.27 instead of 3.33 for the pure stoichiometric composition (calculated with the following charges 2 for Sr and O, 3 for La). This value is compatible with the magnetic and transport performance of the device with the STO barrier 1.5 nm wide.

The profiles of the different cation distributions across the interfaces are very similar: they concern Mn and La in the LSMO layer, Ti in the STO junctions and Sr in both phases Fig. 3a). Their shapes are rather symmetric between the "bottom" and the "top" interfaces, except maybe for the Sr and La profiles which, on the selected profile, seem to display a more extended transition below the "bottom" interface than above the "top" interface (this behaviour will be further discussed in the following paragraph). These results are consistent with a stable composition of the two LSMO layers up to the last atomic planes, within the present limits in spatial resolution and statistical accuracy. When comparing several profiles of the oxygen K signal across the interfaces (see Figs. 3b–d), no reproducible oxygen under-stoichiometry stronger than in the bulk LSMO layers is revealed close to one or the other interfaces, except in the Figure 3b profile.

3.2.3 "2D" mapping of the doping level estimated from the La/Sr ratio

The doping level x can be deduced from the measurement of the concentration ratio in lanthanum and strontium $(1-x)/x$, which should be nominally equal to 2 in the bulk LSMO and go down to 0 in the tunnel barrier (Fig. 4). The slight variations, which may be detected on "1D" profiles such as shown in Figure 4a (diamond-shaped curve), are not sufficiently reproducible to be representative of one of the interfaces. Indeed, the "sum" profile corresponding to the average profile of about fifty spectra (dark dots,

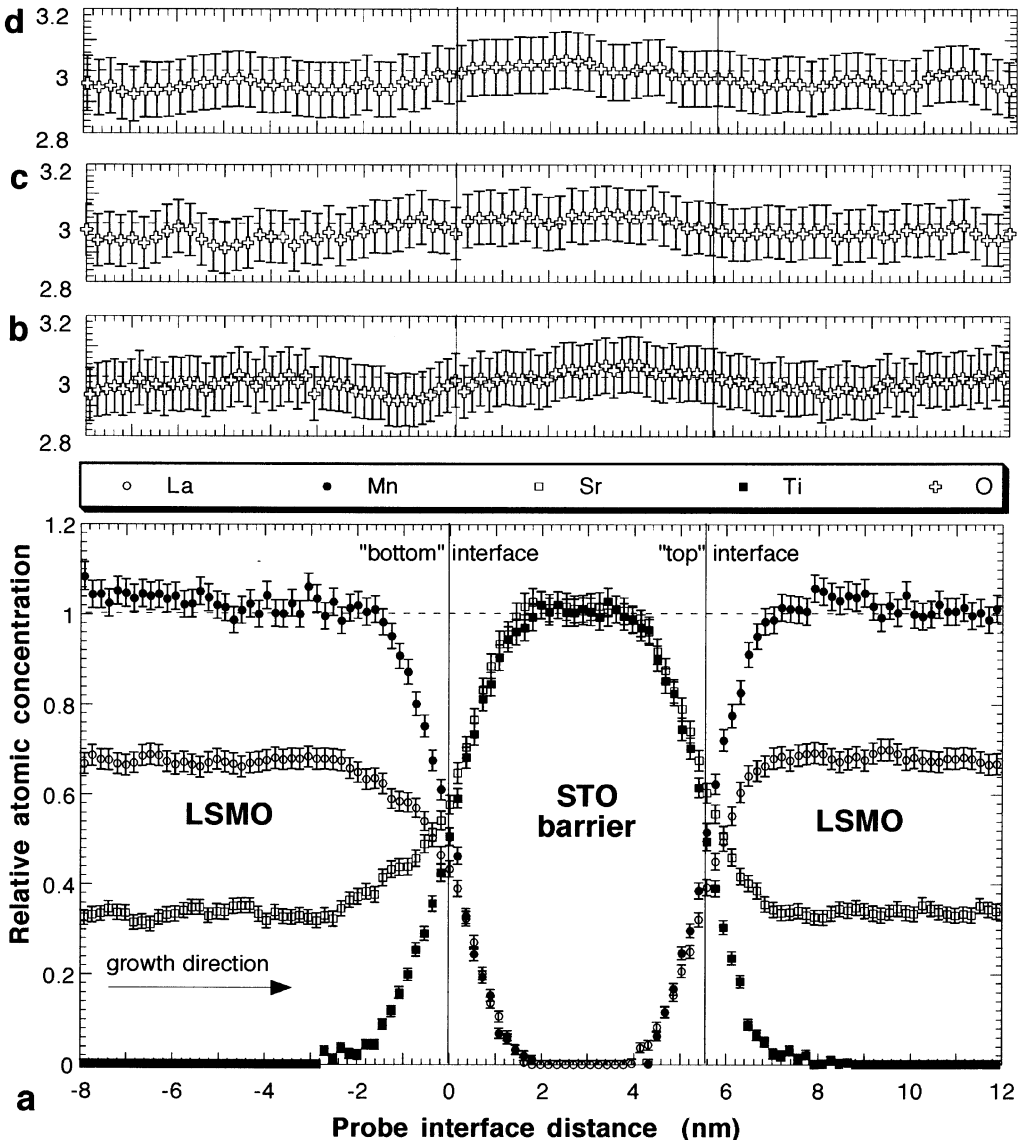

Fig. 3. Relative atomic concentration profiles of the cations (Mn, La, Sr, Ti) and the anion acquired across interfaces LSMO/STO with the STO barrier (5.5 nm wide). (a) and (b) correspond to the same line spectrum as schematically represented in Figure 1. (c) and (d) show two other oxygen profiles. Experimental conditions and data processing are described in Section 2. The acquisition time for each spectrum was 10 ms or 100 ms depending on the corresponding edge.

Fig. 4a) is quite symmetrical. The variations or asymmetry visible in some profiles cancel over about twenty nanometers along the interfaces. Anyway, these variations are very low and close to the nominal value 2 which corresponds to a doping amount of x equal to 0.33. It should reach the down value of 0.66 or the up value of 4 (respectively $x = 0.6$ or 0.2) to have strong negative effects on the magnetic or transport properties. Figure 4b exhibits the La to Sr atomic ratios extracted from a "2D" spectrum-image. This figure is displayed in three dimensions: two for the probe position and a third one for the atomic ratio. These profiles correspond to probe scans acquired perpendicularly to the interface plane. This image reveals the stability of the doping level up to the interfacial zone with the insulating barrier.

3.3 ELNES structure evolution across the interfaces

For these tunnel junctions, the study of the Mn-2p edge at the interfaces allows to determine the Mn valence, which is related to the doping and therefore controls the transport properties. Due to the strong covalent character of the bonding in these compounds, the O-1s edge is the other most relevant signal. The electronic structure of Ti atoms, which substitutes Mn in the insulating barrier has also been checked across the interface area.

3.3.1 Mn-2p edge

As in other transitions metals, the Mn-2p edge appears as made of two white lines corresponding to the

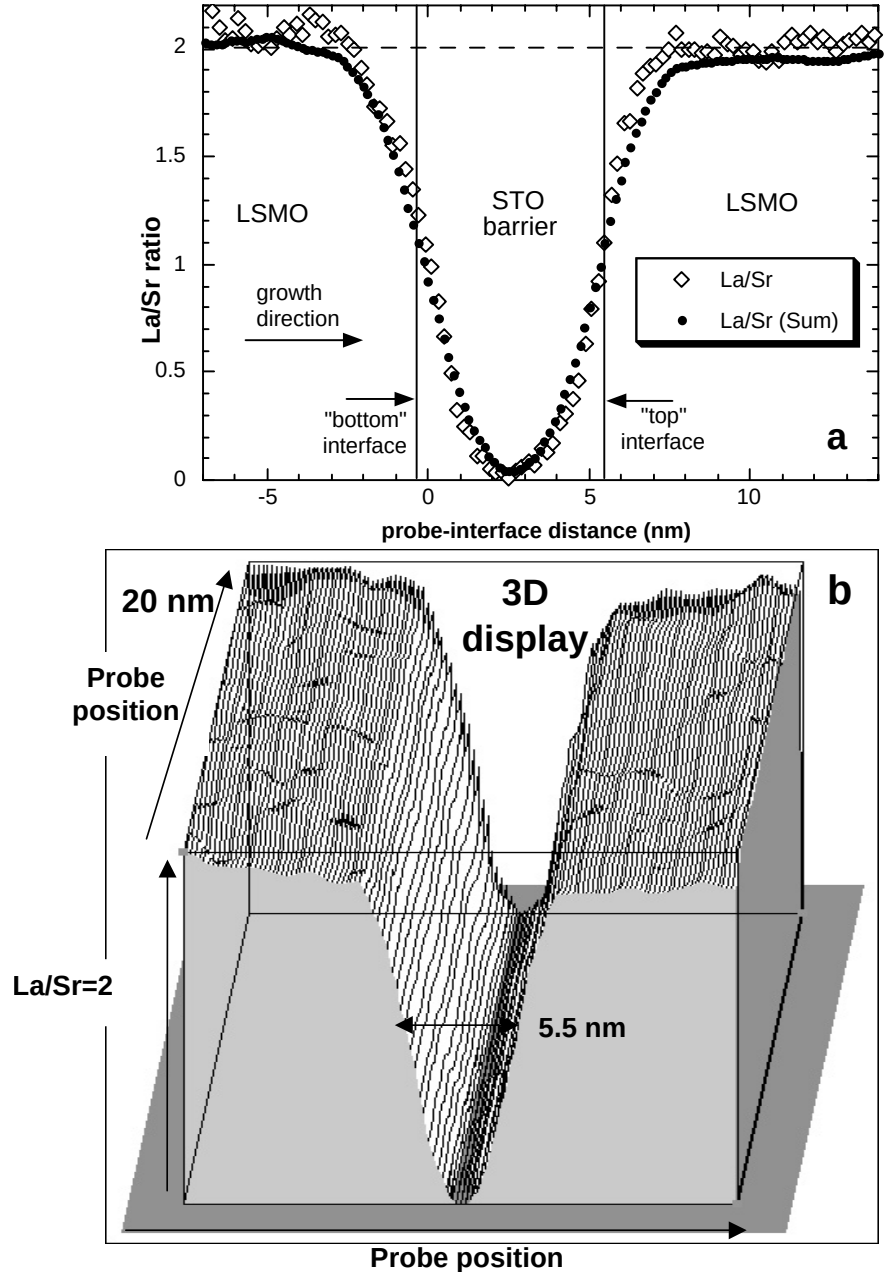

Fig. 4. La to Sr atomic ratio profiles across the LSMO/STO/LSMO interfaces extracted from a "2D" spectrum image (x-y probe scan): (a) one of the profile (diamond-shaped curve) and the profile sum (dark dots curve), (b) the "3D" display of this ratio. STO barrier 5.5 nm wide, 10 ms per spectrum for the acquisition time.

excitation of electrons from $2p$ to $3d$ states, superimposed on a continuum which can be calculated with a Hartree-Slater model. We have measured the position of the maxima of these two white lines at 642 eV (L_3 peak) and 653 eV (L_2 peak) for x equal to 0.33 ($La_{(1-x)}Sr_xMn0_3$) (Fig. 5). These spectra do not exhibit strong outstanding features as one might expect for these spectroscopic features dominated by multiplet effects. However, previous XAS experiments [41] have demonstrated that the broadening of the L_3 and L_2 peaks is not an experimental artefact but is rather of intrinsic origin for these manganites. If the Sr doping is stronger, the L_3 peak is shifted towards higher energy losses as a consequence of changes in the electrostatic energy at the Mn site. The slight shape variation measured between LMO and SMO refers to spectral difference for ground state of primary $3d^3$ and $3d^4$ configuration with various crystal fields (from 1.5 eV to 2.4 eV for $0 \leq x \geq 0.9$) [25,41,42]. The energy shift can be used as a fingerprint to monitor the valence state across the LSMO layer up to the interface with the STO barrier.

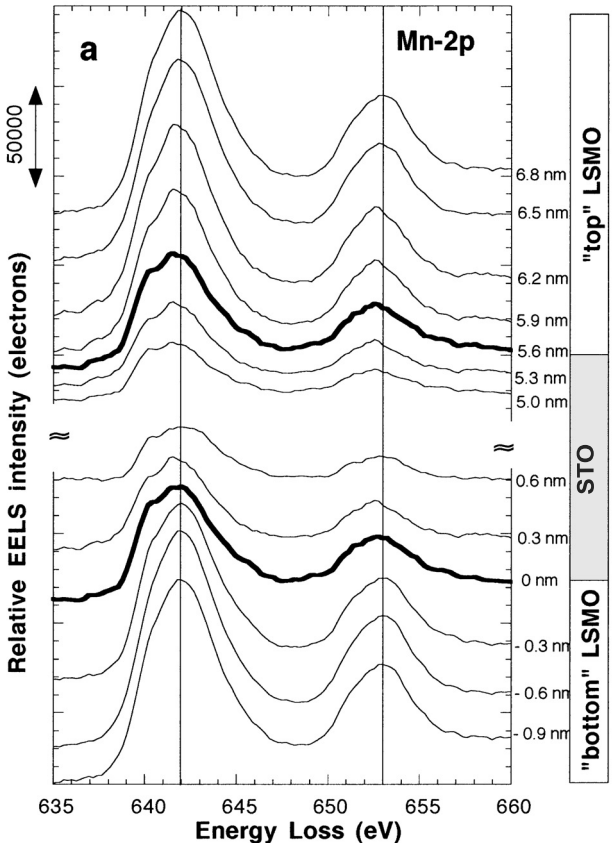

Fig. 5. Variation of the Mn-2p edge across all the interfaces between LSMO and STO: a) interfaces with the STO barrier 5.5 nm wide and b) interface with the STO substrate. EELS line spectrum was used (MSA, no PSF correction). The distances labeled on the figure correspond to the probe-interface distance which is referenced "0 nm" at the apex of the "bottom" interface. The acquisition time for each spectrum was 200 ms.

The L_3/L_2 intensity branching ratio constitutes another indication to monitor the valence in this multilayered system [36,37,43].

The change of the Mn-2p ELNES structures is recorded step by step while crossing the STO barrier (see Fig. 5) using an interface-probe distance step of 0.3 nm. The Mn-2p edge in the "bulk" LSMO layers (displayed on the bottom and on the top of Fig. 5a) is in good agreement with equivalent spectra recorded with XAS [41]. At the apex of the interfaces with the barrier, pointed out in bold characters in Figure 5a, the Mn signal remains sufficiently high (more than 10^6 electrons integrated over 30 eV) to discriminate weak ELNES variations from the experimental noise. A specific fine structure on the L_3 line is detected at the interfaces, marked by a very slight shift towards lower energy losses and a more visible splitting. This specific ELNES, identical at the two interfaces, is present on both kinds of specimen ("thin" and "thick" STO barriers) and is also visible at the interface with the STO substrate (Fig. 5b). It seems to be a very general behaviour, which is further confirmed in 2D spectrum-images acquired with high energy and spatial resolutions. The chemical EELS image (Fig. 6a) corresponds to a Mn map extending over both sides of the insulating barrier. The sequence of Mn-2p edges shown in Figure 6b is extracted from the same spectrum-image data set, when selecting individual spectra corresponding to the different probe positions along one interface shown as an arrow in Figure 6a. A similar observation can be made along the"top" interface. The specific interface structure is more or less pronounced according to the probe location, which could be attributed to the presence of steps along the interfaces as seen in HRTEM images. Within the frame of a pure ionic description, the energy position of the Mn-L_3 peak at these interfaces is not compatible with a valence increase towards Mn^{4+} and a Sr enrichment.

Experimental and theoretical studies have demonstrated that a change in the d band occupancies (due to the formal valence or to charge transfer), in the spin state or in the magnetic ordering may alter the white line ratios of 2p transition metal spectra. All these aspects are important in the case of these multilayered materials. Consequently we have examined with great care the spatial evolution of the L_3/L_2 intensity ratio. Figure 7 shows the results when the probe is scanned across the LSMO layers and the STO barriers ((a) 1.5 nm wide and (b) 5.5 nm wide). Due to the experimental conditions (Sect. 2.2), the accuracy of this extraction is close to 3% in the "bulk" LSMO layers. The ratios calculated for the LMO ($Mn^{"3+"}$) and the "SMO" ($Mn^{"4+"}$) references have also been added as dotted lines. For the LMO reference, the L_3/L_2 ratio corresponds to EELS measurement carried out on our reference sample. For the "SMO" reference ($x = 0.9$), the value is extracted from XAS measurements [41] for $x = 0$ and $x = 0.9$, then normalized to our experimental value for $x = 0$ (LMO). This correction was less than 10% which could be considered as a sign of reliability. From these references, this ratio varies by 14% between Mn^{3+} (LMO) and $Mn^{"4+"}$ ("SMO"). According to the Mn valency in

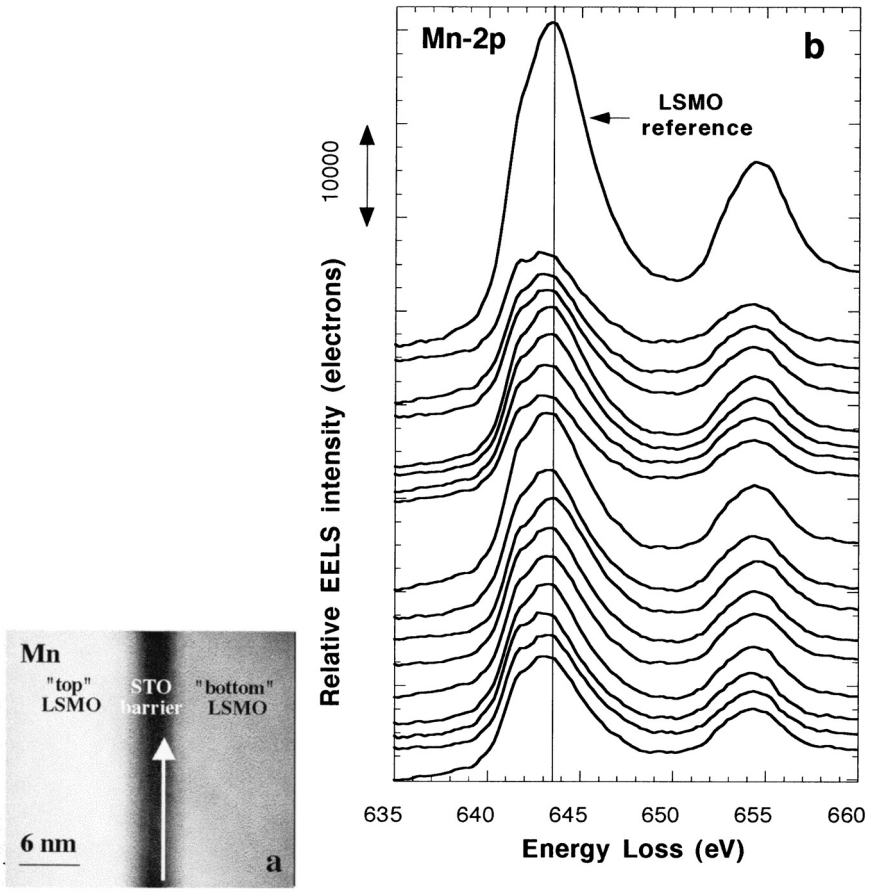

Fig. 6. Variation of the ELNES Mn-2*p* edge acquired in "2D" image spectrum mode: a) Mn map of the selected area. The white row schematically depicts the probe location along the"top" interface corresponding to the spectrum sequence displayed in b). The acquisition time for each spectrum and the total acquisition time were 50 ms and 205 s respectively. No PSF correction is used.

the range 3+ to 4+ and considering the instrumental error (Fig. 7), a linear approximation is sufficient to determine the Mn valency across the LSMO layers. As shown very clearly in Figure 7, the L_3/L_2 ratio in the LSMO layers lies between the values measured for the two references (2.5 for LMO and 2.2 for "SMO") and shows a good stability, with a mean value of 2.40 in both samples. This value roughly corresponds to a mixed valence 0.67 Mn^{3+}+ 0.33 Mn^{4+} which is in agreement with the elemental composition and the measured magnetic and transport properties.

3.3.2 O-1s edge

Unlike manganese, oxygen is present in LSMO as well as in STO with different fine structures. Figure 8 shows a sequence of O-1*s* edges extracted from a line-spectrum acquired when scanning the probe across a tunnel junction. Let us point out the high sensitivity of the technique associated to the very strong signal-to-noise ratio within these individual spectra. Reproducible changes can be detected even with step increments of 0.3 nm in spite of the much larger extent of the probe volume. The ELNES structure of the O-1*s* edge for these systems is usually governed by the hybridisation of 2*p* anion states with 3*d* metal states, forming empty bands of predominantly metal character above the Fermi level [41,44–46]. These features have been identified for the MnO_2 and TiO_2 compounds, which are of rutile type and basically composed of MnO_6 or TiO_6 octahedrons [47]. In LSMO, the "a" feature at 531 eV (Fig. 8) is attributed to overlapping bands of O-2*p* and Mn-3*d* character. In the case of a Sr enrichment (Mn^{3+} to Mn^{4+}), this peak must shift to lower energy losses and a second peak appear at 533 eV [41]. The other structures "b" and "c" can be attributed to the influence of higher energy states like La-5*d* (LSMO), Mn-4*sp* (LSMO), Ti-4*sp* (STO). Considering the changes displayed in Figure 8, there seems to be a continuous variation from the LSMO to the STO phase. As for Mn-2*p*, no trend towards Mn^{4+} corresponding to a Sr enrichment is clearly detected. Contrary to the changes observed on the Mn line at the interface itself, a slight trend towards Mn^{3+} would be very difficult to detect due to the presence of $SrTiO_3$, the corresponding edge of which shifts in the same energy loss direction. The MSA analysis confirms that no new significant spectral feature appears in the interface area, which validates the assumption that the O-1*s* edge corresponds to a linear combination of LSMO and STO fine structures.

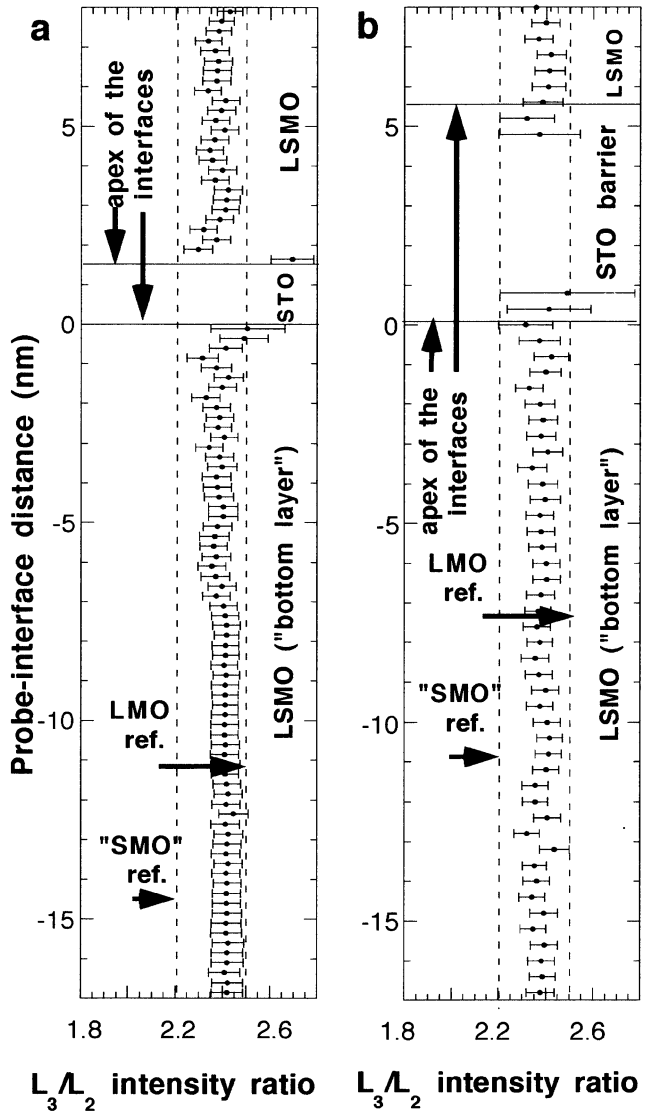

Fig. 7. Variation of the L_3 to L_2 white line intensity ratio of the Mn-2*p* edge as a function of the probe-interface distance for specimens with a STO barrier thickness of a) 1.5 nm and b) 5.5 nm. "0 nm" corresponds to the apex of the "bottom" interface. The reference values of the L_3 to L_2 ratio for the $LaMnO_3$ (LMO) and $La_{0.1}Sr_{0.9}MnO_3$ ("SMO") are mentioned.

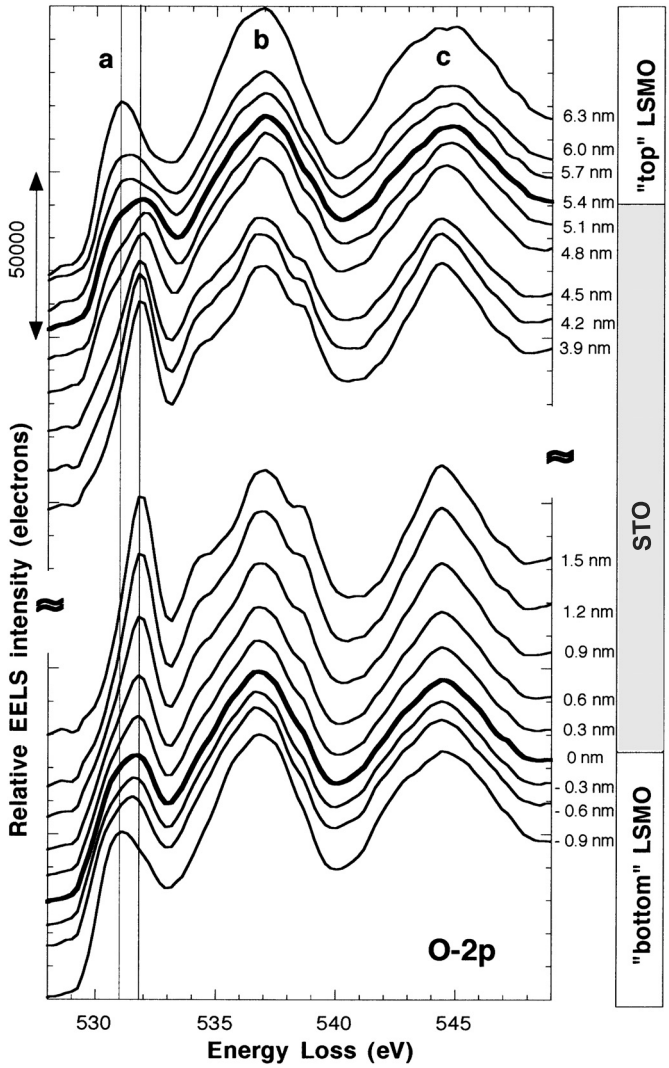

Fig. 8. Evolution of O-1*s* edges across the bottom and the top interfaces between LSMO and STO (specimen with STO layer 5.5 nm wide, after MSA and energy deconvolution technique). The acquisition time for each spectrum was 100 ms.

Mn and Ti atoms occupy similar positions in the LSMO and STO perovskite structures. With or without energy deconvolution technique, no significant variation of the Ti L_{23} lines has ever been detected even at the interfaces.

4 Discussion

The very significant number of acquired data and the corresponding information redundancy lead us to consider these analyses sufficiently representative of the elemental composition and of the electronic states both on the "bulk" type parts of the specimen (LSMO and STO respectively) and at the three interfaces by themselves (STO substrate/ LSMO "bottom" layer, LSMO "bottom" layer/STO tunnel barrier, STO tunnel barrier/LSMO "top" layer). It obviously complement our previous work on the LSMO/STO/Co junction [25].

Let us first summarize the major outputs of the present experimental study:

(i) About quantitative elemental analysis:
- In the "bulk" areas, the average distribution of all cations and oxygen fit rather well to the nominal values of the grown layers, as it can be checked from the established elemental composition formula.
- When compared to its value measured in the STO substrate, the oxygen content in the LSMO layer would correspond to an understoichiometry of about 3%. As a matter of fact,

this oxygen content displays weak variations of an equivalent magnitude across the manganite layers, which are visible in spite of the limited accuracy of the measurements.

- The transition regions at the interfaces are broadened with respect to the nominal size of the incident probe (of the order of 0.7 nm). Similar broadening have also been noticed with the 0.2 nm probe used by Verbeek *et al.* in a comparable study. Several reasons, mostly due to the specimen under investigation, have been proposed to account for these measured larger widths of transition.
- Much attention has been paid to detect if there is any reproducible dissymetry in the elemental composition profiles when analyzing the bottom and top interfaces respectively. If in a few individual line profiles, the top interface seems to be narrower (generally between 1.2 and 1.4 nm in a 20–80 edge measurement as compared to 1.5 to 1.8 values measured at the bottom one), when many profiles are averaged, the behaviour becomes quite symmetrical.
- The doping rate x, which is deduced from the La/Sr atomic concentration ratio, is stable at values between 0.33 and 0.35 over the bulk and close to the interfaces when the La intensity begins to drop to zero. There is no evidence for an increased Sr content in the neighbourhood of the interfaces. Similarly, there is no trend of an increased understoichiometry in the oxygen content in the manganite layers close to the interfaces, as compared to the observed stoichiometry variations detected in the bulk (all of them being of the order of 3 at% maximum).

(ii) About fine structures observations on selected Mn and O edges:

- The weak changes observed in the L_3 and L_2 Mn lines are quite symmetric with respect to the STO junction, when probed with small incremental steps of the probe position (of the order of 0.3 nm perpendicularly to the three different interfaces which have been investigated.
- The major change which has been identified, concerns the fine structure of the L_3 line, as amplified in the second derivative mode shown in Figure 9. It is a shift of the total weight of the line towards lower energy loss values, which is in contradiction with the shift to be expected in the case of an increased valence of the Mn ion (towards higher energy loss values). It is also an increased visibility of the splitting into two components appearing clearly when the probe is at the apex of the interfaces (positions 0 and 5.5 nm in Fig. 9).
- The measured L_3/L_2 branching ratio values always lie between the measured values for the LMO and "SMO" cases. They may be very stable when moving the probe position across a given manganite layer (see for instance the "bottom" layer in the 1.5 nm junction). But it may also exhibit fluctuations which confirm that the LSMO layers by themselves are not perfectly homogeneous in composition. When investigating the neighbourhood of the STO junction, the Mn L_3/L_2 junction seems to increase for the probe positions already positioned within the barrier and probing therefore only the ultimate Mn layers.
- As for the oxygen K-edge, in spite of an excellent signal-to-noise ratio, it does not seem to deviate from a linear combination of a LSMO type behaviour and a STO one. All identified features are in fact very similar to those recorded with XAS on bulk specimens, which display in particular the weak splitting of the prepeak in the LSMO layer and the sharp peak at 531.8 eV in the STO layer.

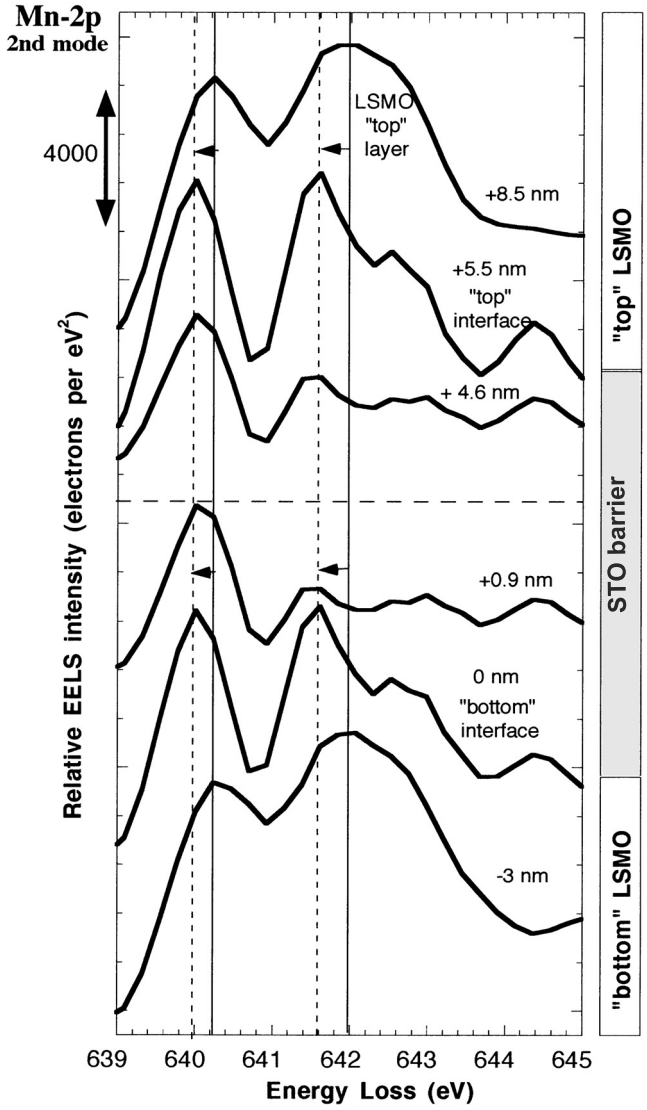

Fig. 9. Change of the Mn-2p edge at the interfaces LSMO/$STO_{barrier}$ displayed in the second derivative mode. The probe position "0 nm" is referenced to the apex of the "bottom" interface. The vertical lines highlight the weak energy shift of edge features at the interfaces ("bulk" and "interface" energy position in full line and dotted line respectively).

All these detailed results are due to the high signal contained in the recorded spectra, which makes that in an oversampling scheme, weak spectral changes can be attributed to changes in position much smaller than the intrinsic dimension of the analysed volume, therefore extending the information range below the spatial resolution. This is also due to the high stability of the probe position during the acquisition times.

Let us point out that the present results are in good agreement with the previous EELS data which we have published on Mn $L_{2,3}$ and O K fine structures recorded on test $La_{1-x}Sr_xMnO_3$ specimens with $x = 0$, 0.33 and 0.9 [25], as well as with the XAS spectra at higher energy resolution published by Abbate *et al.* [41]. In particular both sets of data exhibit a clear shift of the maximum of the Mn L_3 line by 1 eV from the 3+ to the 4+ valency. In their EELS study of SMO/LMO multilayers, [39] show only very weak changes between the Mn lines of the SMO and LMO layers, in contradiction with the other mentioned results. They attribute it to the covalent character of the Mn-O bonds in their specimen.
What can we learn from these measurements?

(i) In our previous EELS study of the Co/STO/LSMO system dealing with only one LSMO/STO interface [25], we had deduced from the observation of a similar behaviour for the Mn L_3 line, that the LSMO should be terminated by a $La_{2/3}Sr_{1/3}O$ atomic layer preserving the local environment and therefore the nominal 3.33 valency of the Mn ion. It was also suggested to consider in detail the case of a reverse LSMO/STO/LSMO junction in order to check whether the sequence of atomic planes would be different at the "bottom" and the"top" LSMO/STO interfaces. A "MnO_2-SrO" termination, richer in Sr in the first neighbouring atoms around the Mn ion, would induce an increase of its valence and the degradation of the junction performance (spin reversal). From the present spectrum sequences across all the LSMO/STO interfaces, a similarity is clearly revealed on the edge features, which does not confirm the previous hypothesis (Figs. 5, 8 and 9). These new analyses therefore suggest that the sequences of atomic planes are identical ("$La_{0.66}Sr_{0.33}O$-TiO_2") or that the electronic structure of the Mn ions is also sensitive to more distant neighbouring cations and anions. This hypothesis of identical sequences also suggests that the surface energies control the atomic plane termination under the thermodynamic conditions during elaboration.

(ii) As for the L_3/L_2 branching ratio, let us consider what can be the reason for its generally observed increase at the apex of the terminating Mn atoms close to the insulating STO barrier. A high to low spin transition is not the cause of this increase in the L_3/L_2 ratio at this interface since spectra for Mn ion with low spin exhibit a smaller L_3/L_2 ratio. It is also quite unlikely that a change in the magnetic ordering of the material might be the reason for that change. It has been shown that the white line ratio may greatly vary (up to 25%) with the magnetic orientation in an X-ray circular magnetic dichroism experiment [42]. However, circular dichroism is almost unpractical in EELS geometry. To our knowledge, X-ray linear dichroism has not been reported for this material, but its intensity would be smaller than in the case of circular polarization. Linear polarization could be achieved in a STEM but its effect is strongly diminished as compared to the X-ray equivalent due to the large convergence angle. For these reasons, we do not believe that a magnetic ordering variation might have been detected by the present EELS experiment at that interface. Therefore, the evolution of the L_3/L_2 intensities is rather related to a change in the d band occupancy than to a magnetic effect (let us also remind that our experiments are performed at room temperature). This interpretation is confirmed by the good correlation observed between the change of the white line ratio and the small chemical shift of the L_3 white line. This latter chemical would not be expected in case of a pure magnetic origin of the L_3/L_2 ratio variation. Within the frame of an ionic description, which is rather well adapted to account for the variations of the branching ratio, an increase of its value up to that measured for the LMO reference (about 2.5) would correspond to an equivalent formal valence reduction down to 3 (instead of 3.33 in the bulk) for the Mn ions, or said in equivalent terms to an increased Mn 3d occupancy at the interface. It can also be attributed to a local understoichiometry in oxygen around the Mn sites, which would reduce the charge transfer from the Mn cation towards its oxygen anion neighbours, consequently enhancing the trend to lower valence character. This character is quite compatible with the weak chemical shift of the L_3 line towards lower energy losses, which has been identified thanks to the increased detection efficiency in the present experiments with respect to the previous ones [25].

(iii) Let us now consider the enhanced splitting of the Mn-L_3 edge, which we have clearly identified in the second energy-derivative mode at the interface between the LSMO layers and the STO barrier. Two major approaches can be referred to, for providing reasonable clues to understand this trend. In an ionic description, the fine structure on these L lines is mostly governed by intra-atomic correlations responsible for the multiplet structure, on which the crystalline symmetry imposed by the neighbouring anions is accounted for by a crystal field parameter 10 Dq. In their paper, Abbate *et al.* [41] show comparisons between experimental Mn $2p$ XAS spectra and simulations performed within this model for the two species with $x = 0$ and 0.9. The agreement is reasonably good. In a covalent model, which should be more appropriate for the Mn oxides (see also the discussion by Kurata and Colliex [37]), the observed changes in fine structures would correspond to changes in density of states and consequently in the filling of the

unoccupied states. If one assumes an extra breakdown of the local octahedral symmetry on the Mn sites, it could induce an extra splitting of Jahn-Teller type [48]. Two reasons may be responsible for such an effect: (i) the first one is the strain of the crystal parameter between LSMO and STO – although the latter one has been identified to be the best substrate for epitaxial growth – of the order of 1% (in tension parallel to the interface and in compression perpendicular to it). This slight structural deformation is also accompanied by a disalignment of the MnO bonds. More extensive diffraction and HREM observations have shown that the angular distorsion needs at least 20 nm to 30 nm to be recovered and that the recovery of the parameter lengths requires much thicker deposits [29]. Consequently, it is quite reasonable to assume that these distorsions may induce a splitting of the *e.g.*↑ band which contains the Fermi level in the metallic state ($0.2 < x < 0.6$), into two sub-bands. Consequently, the filling of these sub-bands could vary across the interface as a consequence of the variable charge transfer; (ii) another likely influential parameter is the rate and ordering of the suspected oxygen vacancies in this transition regions. However, we are presently lacking of more defined atomic level information and consequently of *ab initio* calculations of the involved electronic structure to be able to propose more satisfactory explanations than only a few plausible routes to be further explored. We can however put forward some hints to answer to reasonable objections. If the covalent model is generally more appropriate, it is well known that the information about an eventual degeneracy breakdown in the Mn 3*d* band would be more directly observed on the equivalent prepeak on the oxygen K level as a consequence of the strong *p*-*d* hybridisation. In our experimental situation, we have seen that such a weak effect on the prepeak of the O K edge would be masked by the strong signal coming from the oxygen atoms bound to the Ti ions in the STO layer. Another argument could be to push forward an interpretation in terms of changes in multiplet peak distributions, as for Mn ions in different environments. It is well known however that such a description is much more suitable for Mn fluorides than for Mn oxides, where different contributions mask these multiplet lines, so that the general shape of the Mn L_3 and L_2 lines is rather featureless. The major arguments are the larger Mn d bands and an increased spread of the multiplet distribution induced by the lower symmetry around the Mn ions [41]. To reconciliate both ionic and covalent descriptions, we can finally notice that the best model should be intermediate with a tendency to increased ionicity from SMO to LMO, which is in agreement with all arguments put forward in the previous discussion.

As a summary, we have clearly pointed out in this discussion that the electronic structure on the Mn atomic sites which is explored at high spatial and energy resolution with the presently used spatially resolved EELS techniques, is quite sensitive to its detailed specific environment at the interfaces between the ferromagnetic metallic layers and the insulating paramagnetic STO tunnel barrier. It obviously differs from the bulk one. However, the required detailed interpretation of the ELNES changes at the interface is not available at the present time. It will mix "band structure" and "multiplet" approaches. Calculations of the electronic structure of the atoms in bulk LSMO are already non trivial. Contrary to bulk LCMO [49], no such results exist in the literature for bulk LSMO, to our knowledge.

5 Conclusion

In spite of its limitations, the present study can provide a few clues for a better understanding of the mechanisms, which degrade the device performance. Indeed, the transport properties of the LSMO, optimized for x equal to 0.33, result from several factors induced by the atomic arrangement and the electronic structure. They are in majority due to the presence of carriers (with majority spin↑) at the Fermi level in $La_{0.66}Sr_{0.33}MnO_3$ [2,50]. The chemical shift and the white line ratio change detected at the interfaces in the present study, plead for a weak decrease of the Mn valence in the vicinity of the interface. The small electron doping at the interface may be sufficient to modify the transport properties of the LSMO/STO/LSMO junction. In addition, the Mn-2*p* spectra at the interface exhibit a more resolved splitting of the L_3 line, which may be an indication of structural deformations mostly induced by strain and oxygen vacancies.

The results of this atomic level characterization demonstrate relatively weak changes on atoms at the interfaces with respect to atoms in the bulk. A fundamental question can then be raised: are these changes of sufficient amplitude to be really responsible for the different behaviour in transport properties? It is not surprising as the behaviour of a tunnel junction is highly dependent on the detailed electron state distribution on both sides of the barrier. However, the transport properties are measured for devices of large lateral dimensions and over a large range of temperatures. It would be useful to look for the origin of these changes in macroscopic effects such as the existence of roughness and of shrinkage areas over the important lateral dimensions involved in these devices.

A final message is of more technical character. Such a detailed EELS analysis, together with its identified limitations, pleads for a continuous improvement in instrumentation capabilities and performance. The first one is the systematic use of the "2D" spectrum image mode. It provides collections of many high energy resolution spectra extending over quite different energy windows (the information is distributed into many different signals at quite variable energy losses) and acquired over many pixels of interest across the junction. The second one is the support of well adapted numerical processing techniques to optimism the extraction of useful information, in particular the Multivariate Statistical Analysis and the

introduction of spectral deconvolution methods for improving energy resolution. The last one is the clear identification of the limit imposed by the present probe size. It further stimulates the need of using nanoprobes with a diameter equal or less than one atom size (as already demonstrated by [51]), in channelling conditions for the selection of an information localised at the apex of identified atomic columns.

The authors wish to thank F. Studer (CRISMAT, Caen, France) for the calibrated LMO specimen and acknowledge the CNRS/DGRST convention for a financial support of L. Samet at LPS-Orsay.

References

1. H.L. Ju, H.-C. Sohn, K.M. Krishnan, Phys. Rev. Lett. **79**, 3230 (1997)
2. T. Saitoh, A.E. Bocquet, T. Mizokawa, H. Namatame, A. Fujimori, Phys. Rev. B **51**, 13942 (1995)
3. C. Zener, Phys. Rev. **82**, 403 (1951)
4. P.G. de Gennes, Phys. Rev. B **118**, 141 (1960)
5. J.-M De Teresa, A. Barthélémy, A. Fert, J.-P. Contour, F. Montaigne, P. Seneor, Science **286**, 507 (1999)
6. A. Fert, *et al.*, Materials. Sci. Engineering B **84**, 1 (2001)
7. J.S. Noh, T.K. Nath, C.B. Eom, J.Z. Sun, W. Tian, X.Q. Pan, Appl. Phys. Lett. **79**, 233 (2001)
8. Y. Lu, X.W. Li, G.Q. Gong, Gang Xiao, A. Guptaz, P. Lecoeur, J.Z. Sun, Y.Y. Wang, V.P. Dravid, Phys. Rev. B **54**, 8357 (1996)
9. M. Viret, M. Drouet, J.-P. Contour, J. Nassar, C. Fermon, A. Fert, Europhys. Lett. **39**, 545 (1997)
10. J. Nassar, M. Viret, M. Drouet, J.-P. Contour, C. Fermon, A. Fert, Mat. Res. Soc. Symp. Proc. **494**, 231 (1998)
11. E. Favre-Nicolin, L. Ranno, C. Dubourdieu, M. Rosina, Thin Solid Films. **400**, 165 (2001)
12. M. Viret, L. Ranno, J.M.D. Coey, J. Appl. Phys. **81**, 4964 (1997)
13. M. Bibes, Ll. Balcells, S. Valencia, S. Sena, B. Martinez, J. Fontcuberta, J. of Appl. Phys. **89**, 6686 (2001)
14. M. Bibes, M.J. Casanove, Ll. Balcells, S. Valencia, B. Martinez, J.C. Ousset, J. Fontcuberta, Appl. Surf. Sci. **188**, 202 (2002)
15. M. Viret, J. Nassar, M. Drouet, J.-P. Contour, C. Fermon, A. Fert, J. Magn. Magn. Mater. **198-199**, 1 (1999)
16. M. Izumi, Y. Konishi, T. Nishihara, S. Hayashi, M. Shinohara, M. Kawasaki, Y. Tokura, Appl. Phys. Lett. **73**, 2497 (1998)
17. R. Bertacco, M. Portalupi, M. Marcon, L. Duo, F. Ciccacci, M. Bowen, J.-P. Contour, A. Barthélémy, J. Magn. Magn. Mater. **242**, 710 (2002)
18. R. Bertacco, J.-P. Contour, A. Barthélémy, J. Olivier, Surf. Sci. **511**, 366 (2002)
19. H.Y. Hwang, S.W. Cheong, N.P. Ong, B. Batlogg, Phys. Rev. Lett. **77**, 2041 (1996)
20. J.M. Teresa, A. Barthélémy, A. Fert, J.-P. Contour, R. Lyonnet, F. Montaigne, P. Seneor, A. Vaurès, Phys. Rev. Lett. **82**, 4288 (1999)
21. J.-L. Maurice, R. Lyonnet, J.-P. Contour, J. Magn. Magn. Mater. **211**, 91 (2000)
22. F. Pailloux, R. Lyonnet, J.-L. Maurice, J.-P. Contour, Appl. Surf. Sci. **177**, 263 (2001)
23. J.-L. Maurice, F. Pailloux, A. Barthélémy, A. Rocher, O. Durand, R. Lyonnet, J.-P. Contour, Appl. Surf. Sci. **188**, 176 (2002)
24. O.I. Lebedev, J. Verbeeck, G. Van Tendeloo, S. Amelinckx, F.S. Razavi, H.-U. Habermeier, Phil. Mag. A **81**, 2865 (2001)
25. F. Pailloux, D. Imhoff, T. Sikora, A. Barthélémy. J.-L. Maurice, J.-P. Contour, C. Colliex, A. Fert, Phys. Rev. B **66**, 14417 (2002)
26. J. Benedict, R. Anderson, S. Klepeis, M. Chaker, Mater. Res. Soc. Symp. Proc. **199**, 189 (1990)
27. P. Stadelman, Ultramicroscopy **21**, 131 (1987)
28. J.-L. Maurice, F. Pailloux, D. Imhoff, N. Bonnet, L. Samet, A. Barthélémy, J.-P. Contour, C. Colliex, A. Fert (accepted, Eur. Phys. J AP)
29. J.-L. Maurice, F. Pailloux, A. Barthélémy, O. Durand, D. Imhoff, R. Lyonnet, A. Rocher, J.-P. Contour (accepted, Phil. Mag.)
30. Spectrometer modified at Laboratoire "Physique des Solides" in Orsay by Marcel Tencé and Paul Ballongue
31. C. Jeanguillaume, C. Colliex, Ultramicroscopy **28**, 252 (1989)
32. R.F. Egerton, *Electron Energy Loss Spectroscopy in Electron Microscope* (Plenum Press NY, 1986)
33. N. Bonnet, N. Brun, C. Colliex, Ultramicroscopy **77**, 97 (1999)
34. P. Trebbia, N. Bonnet, Ultramicroscopy **34**, 165 (1990)
35. A. Gloter, A. Douiri, M. Tencé, C. Colliex, Ultramicroscopy **96** (3-4), 385 (2003)
36. T. Manoubi, M. Tencé, M.G. Walls, C. Colliex, Microsc. Microanal. Microstruct. **1**, 23 (1990).
37. H. Kurata, C. Colliex, Phys. Rev. B **48**, 2102 (1993)
38. J. Verbeek, O.I. Lebedev, G. Van Tendeloo, J. Silcox, B. Mercey, M. Hervieu, A.M. Haghin-Gosnet, Appl. Phys. Lett. **79**, 2037 (2001)
39. J. Verbeeck, O.I. Lebedev, G. Van Tendeloo, B. Mercey, Phys. Rev. B **66**, 184426 (2002)
40. C. Prunier-Mory, Ph.D. Thesis, Paris-Sud Univ. (1985)
41. M. Abbate, F.M.F. de Groot, J.C. Fuggle, A. Fujimori, O. Strebel, F. Lopez, M. Domke, G. Kaindl, G.A. Sawatzky, M. Takano, Y. Takeda, H. Eisaki, S. Uchida, Phys. Rev. B **46**, 4511 (1992)
42. E. Pellegrin, L.H. Tjeng, F.M.F. de Groot, R. Hesper, G.A. Sawatzky, Y. Moritomo, Y. Tokura, J. Electron Spectroscopy Related Phenomena **86**, 115 (1997)
43. Z.L. Wang, J.Z. Yin, Y.D. Zhang, W.D. Mo, J. Phys. Chem B **101**, 6793 (1997)
44. F.M.F. de Groot, Ph.D. Thesis, University of Nijmegen, Toernooveld, 6525 ED Nijmegen, The Netherlands (1991)
45. Shang-Di Mo, W.Y. Ching, M.F. Chisholm, G. Dusher, Phys. Rev. B **60**, 2416 (1999)
46. M. Grioni, M.T. Czyzyk, F.M.F. de Groot, J.C. Fuggle, B.E. Watts, Phys. Rev. B **39**, 4886, (1990)
47. H. Kurata, E. Lefevre, C. Colliex, R. Brydson, Phys. Rev. B **47**, 13763 (1993)
48. H.A. Jahn, E. Teller, Proc. Roy. Soc. (London) A **164**, 117 (1938)
49. E. Warren, W.E. Picket, D.J. Singh, Phys. Rev. B **53**, 1146 (1996)
50. A. Chainani, M. Mathew, D.D. Sarma, Phys. Rev. B **47**, 15397 (1993)
51. P.E. Batson, N. Delby, O.L. Krivanek, Nature **418**, 617 (2002)